BIOCHEMISTRY
including biophysical chemistry & molecular biology

Article

pubs.acs.org/biochemistry

Binding Energy and Catalysis by D-Xylose Isomerase: Kinetic, Product, and X-ray Crystallographic Analysis of Enzyme-Catalyzed Isomerization of (*R*)-Glyceraldehyde

Maria M. Toteva,[†] Nicholas R. Silvaggi,[‡] Karen N. Allen,[§] and John P. Richard*[,†]

[†]Department of Chemistry, University at Buffalo, SUNY, Buffalo, New York 14260-3000, United States

[‡]Department of Chemistry and Biochemistry, University of Wisconsin−Milwaukee, Milwaukee, Wisconsin 53201-0413, United States

[§]Department of Chemistry, Boston University, Boston, Massachusetts 02215-2521, United States

ABSTRACT: D-Xylose isomerase (XI) and triosephosphate isomerase (TIM) catalyze the aldose−ketose isomerization reactions of D-xylose and D-glyceraldehyde 3-phosphate (DGAP), respectively. D-Glyceraldehyde (DGA) is the triose fragment common to the substrates for XI and TIM. The XI-catalyzed isomerization of DGA to give dihydroxyacetone (DHA) in D_2O was monitored by ^1H nuclear magnetic resonance spectroscopy, and a k_{cat}/K_m of 0.034 M^{-1} s^{-1} was determined for this isomerization at pD 7.0. This is similar to the k_{cat}/K_m of 0.017 M^{-1} s^{-1} for the TIM-catalyzed carbon deprotonation reaction of DGA in D_2O at pD 7.0 [Amyes, T. L., O'Donoghue, A. C., and Richard, J. P. (2001) *J. Am. Chem. Soc. 123*, 11325−11326]. The much larger activation barrier for XI-catalyzed isomerization of D-xylose (k_{cat}/K_m = 490 M^{-1} s^{-1}) versus that for the TIM-catalyzed isomerization of DGAP ($k_{cat}/K_m = 9.6 \times 10^6$ M^{-1} s^{-1}) is due to (i) the barrier to conversion of cyclic D-xylose to the reactive linear sugar (5.4 kcal/mol) being larger than that for conversion of DGAP hydrate to the free aldehyde (1.7 kcal/mol) and (ii) the intrinsic binding energy [Jencks, W. P. (1975) *Adv. Enzymol. Relat. Areas Mol. Biol. 43*, 219−410] of the terminal ethylene glycol fragment of D-xylose (9.3 kcal/mol) being smaller than that of the phosphodianion group of DGAP (~12 kcal/mol). The XI-catalyzed isomerization of DGA in D_2O at pD 7.0 gives a 90% yield of [1-^{1}H]DHA and a 10% yield of [1-^{2}H]DHA, the product of isomerization with incorporation of deuterium from solvent D_2O. By comparison, the transfer of ^3H from the labeled hexose substrate to solvent is observed only once in every 10^9 turnovers for the XI-catalyzed isomerization of [2-^{3}H]glucose in H_2O [Allen, K. N., Lavie, A., Farber, G. K., Glasfeld, A., Petsko, G. A., and Ringe, D. (1994) *Biochemistry 33*, 1481−1487]. We propose that truncation of the terminal ethylene glycol fragment of D-xylose to give DGA results in a large decrease in the rate of XI-catalyzed isomerization with hydride transfer compared with that for proton transfer. An ultra-high-resolution (0.97 Å) X-ray crystal structure was determined for the complex obtained by soaking crystals of XI with 50 mM DGA. The triose binds to XI as the unreactive hydrate, but ligand binding induces metal cofactor movement and conformational changes in active site residues similar to those observed for XI·sugar complexes.

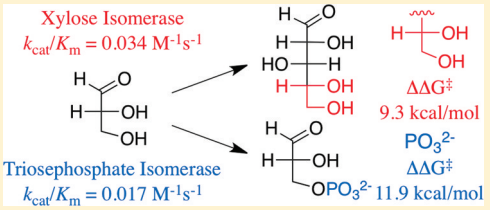

Two mechanisms have evolved for the enzyme-catalyzed isomerization of α-hydroxyaldehydes (aldoses) to give α-hydroxyketones (ketoses). Isomerization of sugar phosphates, as exemplified by conversion of D-glyceraldehyde 3-phosphate (DGAP) to give dihydroxyacetone phosphate catalyzed by triosephosphate isomerase [TIM (Scheme 1A)],[1−8] proceeds

Scheme 1

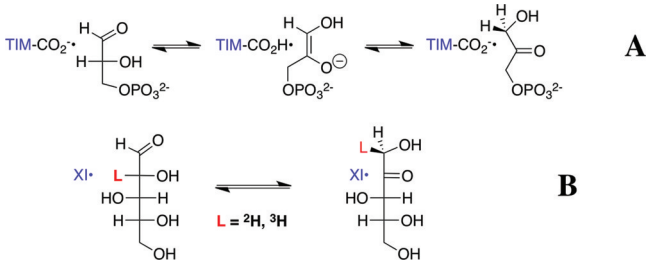

by a proton transfer mechanism through an enediolate intermediate,[8,9] while isomerization of sugars, as exemplified by reactions catalyzed by D-xylose isomerase [XI (Scheme 1B)],[10−16] proceeds by intramolecular hydride transfer. By comparison, the general base-catalyzed isomerization of triosephosphates in water proceeds by a proton transfer reaction mechanism,[17,18] while competing proton and hydride transfer reaction pathways are observed for the nonenzymatic isomerization of glyceraldehyde to give dihydroxyacetone (DHA) in an alkaline aqueous solution.[19,20]

TIM satisfies at least two criteria for perfection in enzymatic catalysis,[3] the most important being that the second-order rate constant (k_{cat}/K_m) of 2×10^8 M^{-1} s^{-1} for isomerization of the free carbonyl form of the substrate is close to the maximum possible for a diffusion-limited reaction (see ref 21).[a] By comparison, the k_{cat}/K_m of ≈10^3 M^{-1} s^{-1} for the XI-catalyzed isomerization of D-xylose[22−24] falls far short of the limiting rate constant of ~10^8 M^{-1} s^{-1} for a diffusion-limited reaction

Received: August 31, 2011
Revised: October 8, 2011
Published: October 13, 2011

catalyzed by a perfect enzyme.[3] We are interested in understanding how this difference in catalytic efficiency is related to the difference in the structure of the substrates of the TIM- and XI-catalyzed isomerization reactions.[15,25]

Truncation of the phosphoryl dianion from DGAP or the terminal $CH(OH)CH_2OH$ fragment from D-xylose gives D-glyceraldehyde (DGA), the fragment common to the substrates for the two enzymes (Scheme 2). TIM catalyzes the slow

Scheme 2

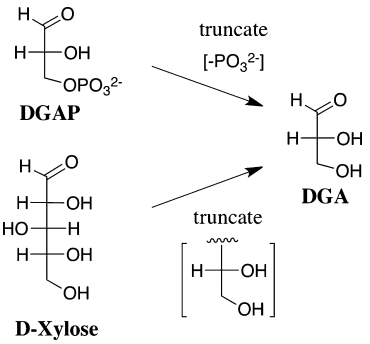

isomerization of the free carbonyl form of DGA to give DHA in D_2O with a k_{cat}/K_m of 0.34 M^{-1} s^{-1} that is much smaller than the k_{cat}/K_m of 2×10^8 M^{-1} s^{-1} for isomerization of DGAP, and only marginally larger than the k_B of 6.5×10^{-3} M^{-1} s^{-1} for deprotonation of DGA by the small Brønsted base 3-quinuclidinone (see ref 26).[a] We report here that the observed kinetic parameter k_{cat}/K_m for the XI-catalyzed isomerization of DGA to give DHA in D_2O is similar to that for the TIM-catalyzed isomerization under the same reaction conditions.[26] The greater efficiency of TIM compared to that of XI for catalysis of the reaction of their whole substrates is therefore related to a difference in the activation of the respective enzymes by interactions with the nonreacting phosphodianion of DGAP and the terminal ethylene glycol fragment of D-xylose, respectively.

We have complemented these kinetic studies with the report of an ultra-high-resolution (0.97 Å) X-ray crystal structure of the XI·triose complex obtained by soaking crystals of XI with DGA. This X-ray crystal structure shows that the more abundant (95% of total DGA) hydrate of DGA (DGAH) was bound to XI. By contrast, TIM shows selectivity for binding and catalysis of the reactive free carbonyl form of the substrate DGAP.[27] The formation of the complex of XI with the unreactive hydrated triose induces movement of the metal cofactor and associated shifts in the position of active site residues that are remarkably similar to the conformational changes observed for complexes of XI with pentose and hexose sugar substrates.

MATERIALS AND METHODS

Materials. Reagent grade organic chemicals and inorganic salts from commercial sources were used without further purification. Water was distilled and then passed through a Milli-Q water purification system. Deuterium oxide (99.9 atom % D), deuterium chloride (35% w/w, 99.5 atom % D), and CD_3COOD (99.5 atom % D) were purchased from Cambridge Isotope Laboratories. D-Glyceraldehyde (90 wt % in water) was purchased from Aldrich. NADH (disodium salt), D-xylose, D-fructose, and sorbitol dehydrogenase from sheep liver (lyophilized powder) were purchased from Sigma. A crystalline suspension of D-xylose isomerase from *Streptomyces rubiginosus* was purchased from Hampton Research. D-Threonohydroxamic acid was prepared by a published procedure.[28]

General Methods. Imidazole and NaCl were dried in a vacuum oven overnight before preparation of buffered solutions in D_2O. pD values were determined via addition of 0.40 to the observed reading of the pH meter at 25 °C.[29] Stock solutions (2 M) of D-xylose and D-fructose in D_2O at I = 0.1 (NaCl) were kept at room temperature for 1 day to ensure formation of an equilibrium mixture of sugar anomers. Commercial D-glyceraldehyde (90 wt % in water) exists mainly as the dimer. This was dissolved in D_2O; the D_2O was removed in vacuo, and the compound was then dissolved in 0.1 M NaCl in D_2O to give an ~50 mM solution at I = 0.1 (NaCl). This solution was kept at room temperature for ≥1 week, until ≥95% of monomeric glyceraldehyde was observed by ^1H NMR analysis. ^1H NMR showed the presence of only ~0.04% DHA. Solutions of authentic DHA [50 mM at I = 0.1 (NaCl)] were prepared in D_2O and were used on the day that they were prepared.

Enzymes were dialyzed against the appropriate buffer at 5 °C. Crystalline XI used in kinetic studies was freed of ammonium sulfate by extensive dialysis against 30 mM imidazole buffer in H_2O (pH 7.0 or 8.0) that contained 12.5 mM $MgCl_2$ [I = 0.1 (NaCl)]. The protein was then dialyzed exhaustively against 30 mM imidazole buffer in D_2O (pD 7.0 or 8.0) that contained 12.5 mM $MgCl_2$ at I = 0.1 (NaCl). Typically, a 3−4-fold volume excess of dialysis buffer over sample was used, and the buffer was changed seven times. The concentration of XI in stock solutions used for kinetic and product studies was determined from the absorbance at 280 nm using an ε of 0.96 mg^{-1} mL cm^{-1} [30] and a monomer molecular mass of 43000 Da.[23] The concentration of XI in stock solutions used for crystallization studies was determined using the Bio-Rad (Hercules, CA) protein assay. Sorbitol dehydrogenase was dialyzed against 30 mM imidazole buffer in D_2O (pD 7.0 or 8.0) that contained 12.5 mM $MgCl_2$ [I = 0.1 (NaCl)]. The enzyme was stable (<5% loss of activity) at 5 °C for more than 6 weeks. One unit of enzyme activity is defined as the amount of enzyme that will catalyze the transformation of 1 μmol of substrate per minute under our assay conditions at 25 °C.

Enzyme Assays. Enzyme assays were performed at 25 °C. The activity of sorbitol dehydrogenase in D_2O was determined by monitoring the enzyme-catalyzed oxidation of NADH by D-fructose at 340 nm. The standard assay solution (1.0 mL) contained 100 mM D-fructose, 0.15 mM NADH, 10 mM $MgCl_2$, and 0.06 unit of sorbitol dehydrogenase in 24 mM imidazole buffer at pD 7.0 or 8.0 [I = 0.1 (NaCl)]. XI was assayed in D_2O by coupling the isomerization of D-xylose to the reduction of the product D-xylulose by NADH using sorbitol dehydrogenase. The standard assay solution (1.0 mL) contained 50 mM D-xylose, 0.23 mM NADH, 10 mM $MgCl_2$, 0.012 unit of XI, and 0.6 unit of sorbitol dehydrogenase in 24 mM imidazole buffer at pD 7.0 or 8.0 [I = 0.1 (NaCl)].

X-ray Crystallographic Analysis. XI from *S. rubiginosus* was prepared for crystallization by overnight dialysis of the commercial crystalline suspension (Hampton Research, Inc.) against 4 L of distilled H_2O followed by concentration to 20 mg/mL using an Amicon centrifugal concentrator (Millipore, Inc.) with a 10000 molecular weight cutoff membrane. XI was

crystallized by the vapor diffusion method with hanging drop geometry over wells containing a solution of 0.2−0.3 M magnesium formate at pH 7.0. Large crystals (~0.4 mm × ~0.4 mm × ~0.2 mm) were obtained after growth at room temperature (~22 °C) for 2 days. The structure of the complex of XI with D-glyceraldehyde was obtained by soaking crystals of unliganded XI for 9 h in a solution containing 0.4 M magnesium formate and 50 mM DGA. Crystals were transferred sequentially to solutions containing 0.4 M magnesium formate, 50 mM DGA, and 5, 15, or 30% 2-methyl-2,4-pentanediol (MPD) and flash-cooled in a gaseous N_2 stream at 100 K. Diffraction data were collected at the National Synchrotron Light Source (NSLS), beamline X12B, using an ADSC Quantum 4 CCD detector. The data were integrated and scaled using DENZO and SCALEPACK.[31]

Model Refinement. The initial phases were derived from the 1.5 Å resolution structure of the unliganded *S. rubiginosus* enzyme [Protein Data Bank (PDB) entry 1OAD][32] in space group $P2_12_12_1$. The coordinates of the unliganded enzyme were used as the search model in determining the orientation of the molecule in the *I*222 unit cell with EPMR.[33] Once the initial phases had been obtained, the structure was refined to 1.5 Å resolution using CNS.[34] Solvent molecules that showed reasonable hydrogen bond distances from and geometry with donor and acceptor atoms were added. Care was taken to avoid modeling the density for the bound ligands as solvent. After the water structure had been deemed to be satisfactory and R_{cryst} had reached approximately 19% (~21% R_{free}), further refinement was conducted using SHELX-97.[35] Following isotropic refinement at full resolution, the model was refined anisotropically. Refinement of the individual anisotropic displacement parameters resulted in a 5.3% decrease in R_{free}. Comparable decreases in R_{cryst} accompanied the changes in R_{free}. Iterative cycles of fitting in COOT[36] followed by refinement in SHELXL continued until the *R* factors converged. At this point, all protein hydrogen atoms except for amino and hydroxyl hydrogens were added using the riding model in SHELXL. This led to an ~1% decrease in R_{free}.

^{1}H NMR Analyses. ^{1}H NMR spectra at 500 MHz were recorded at 25 °C using a Varian Unity Inova spectrometer with a 90° pulse angle, a 6000 Hz sweep width, a 4−6 s acquisition time, and a relaxation delay between pulses of 120 s, as described in our previous work.[20,26,37,38] Normalized areas of the peaks corresponding to a single proton of DGA (A_{DGA}), *h*-DHA ($A_{h\text{-DHA}}$), and *d*-DHA ($A_{d\text{-DHA}}$) in mixtures of these compounds were determined from the integrated areas of the peaks due to the C-1 proton of DGA hydrate (f_{hyd} = 0.95) and the protons due to the free keto forms of *h*-DHA and *d*-DHA (f_{hyd} = 0.16), respectively, as described previously.[20] The concentration of DGA was determined relative to the known concentration of the imidazole buffer from the ratio of the peak areas for the C-4 and C-5 protons of imidazole and the C-1 proton of DGA hydrate using an f_{hyd} of 0.95 for the fraction of DGA present as the hydrate in D_2O.[20,26] A similar method was used to determine the concentration of D-threonohydroxamic acid using the peak area for its C-2 proton.

Reactions of DGA and DHA Monitored by ^{1}H NMR Spectroscopy. The XI-catalyzed reactions of DGA and DHA in D_2O at pD 7.0 or 8.0 in the presence of 24 mM imidazole buffer and 10 mM $MgCl_2$ at 25 °C and *I* = 0.1 (NaCl) were monitored by ^{1}H NMR spectroscopy. The reactions (10 mL volume) were initiated by making a 5-fold dilution of an ~50 mM stock solution of DGA or DHA [*I* = 0.1 (NaCl)] into 30 mM imidazole buffer [*I* = 0.1 (NaCl)] containing 12.5 mM $MgCl_2$ to give final concentrations of 11 mM substrate, 24 mM imidazole, 10 mM $MgCl_2$, and 0.30 mM XI for the reaction at pD 7.0 and 0.20 mM XI for the reaction at pD 8.0. At timed intervals, an aliquot (1 mL) was withdrawn and the solution was adjusted to pD ≈5 with 10 or 25 μL of 1 M CD_3COOD for reactions at pD 7.0 or 8.0, respectively. It was shown in control experiments that this decrease in pD effectively quenches the slow XI-catalyzed reaction. The enzyme was removed by ultrafiltration at 5 °C using a Microcon YM-10 centrifugal filtration device. The filtrate was then flash-frozen over solid CO_2 and stored at −15 °C. ^{1}H NMR analyses of the mixture were performed within 1 week of freezing. It has been shown that DGA is stable to nonenzymatic isomerization and deuterium exchange reactions over this period of time.[20] The same procedure was used to monitor the XI-catalyzed isomerization of DGA in the presence of the competitive inhibitor D-threonohydroxamic acid at 0.5 mM.[28]

The fraction of DGA converted to DHA, $(f_{DHA})_{tot}$, during reaction of ≤10% of the starting DGA was calculated from the normalized peak areas due to a single proton of the reactant, A_{DGA}, and the two products using eq 1

$$(f_{DHA})_{tot} = \frac{A_{h-DHA} + A_{d-DHA}}{A_{DGA} + A_{h-DHA} + A_{d-DHA}} \quad (1)$$

where $A_{h\text{-DHA}}$ and $A_{d\text{-DHA}}$ are the normalized peak areas for a single proton of products *h*-DHA and *d*-DHA, respectively, determined as described previously (see above).[20] The apparent first-order rate constants for the XI-catalyzed conversion of DGA to *h*-DHA and *d*-DHA, k_{obsd} (s^{-1}), were then calculated as the slopes of plots of $(f_{DHA})_{tot}$ versus time according to eq 2

$$(f_{DHA})_{tot} = k_{obsd}t \quad (2)$$

which were linear over the initial 10% of the reaction (see Figure 1). The ratio of the yields of *h*-DHA and *d*-DHA was obtained using eq 3

$$\frac{[d\text{-DHA}]}{[h\text{-DHA}]} = \frac{4A_{CHD}}{A_{CH2} - 2A_{CHD}} \quad (3)$$

where A_{CH2} is the observed area of the singlet at 4.300 ppm due to the α-CH_2OD groups of the free carbonyl form of both *h*-DHA and *d*-DHA and A_{CHD} is the area of the 0.024 ppm upfield-shifted triplet due to the single α-CHDOD group of *d*-DHA (see Figure 2).[20] The fraction of the total DHA product labeled with deuterium, $f_{d\text{-DHA}}/(f_{DHA})_{tot}$, was then calculated from this ratio using eq 4.

$$\frac{f_{d\text{-DHA}}}{(f_{DHA})_{tot}} = \frac{[d\text{-DHA}]/[h\text{-DHA}]}{1 + [d\text{-DHA}]/[h\text{-DHA}]} \quad (4)$$

The slow uncatalyzed reaction of DGA in the absence of XI in D_2O at pD 7.0 in the presence of 24 mM imidazole buffer and 10 mM $MgCl_2$ at 25 °C and *I* = 0.1 (NaCl) was followed directly by ^{1}H NMR spectroscopy[26] by monitoring the decrease in the area of the doublet due to the C-1 proton of DGA hydrate, using the signals for the C-4 and C-5 hydrogens of imidazole as an internal standard.[26] The observed first-order rate constant for this nonenzymatic reaction of DGA, $(k_N)_{app}$, was determined as the slope of a semilogarithmic plot of the fraction of remaining substrate versus time.

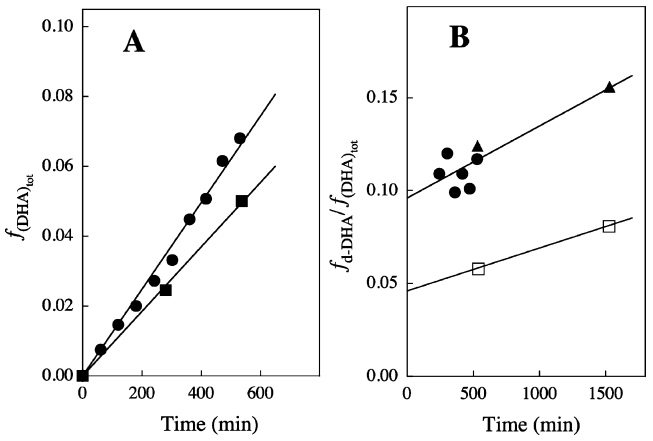

Figure 1. Data for the XI-catalyzed isomerization reaction of 11 mM DGA to give DHA in D_2O in the presence of 24 mM imidazole buffer and 10 mM $MgCl_2$ at 25 °C and I = 0.1 (NaCl) monitored by ^1H NMR spectroscopy. (A) Time course for the fractional formation of total DHA where $(f_{DHA})_{tot}$ was determined from the area of the signals for products *h*-DHA and *d*-DHA and the remaining substrate using eq 1: (●) reaction catalyzed by 0.30 mM XI at pD 7.0 and (■) reaction catalyzed by 0.20 mM XI at pD 8.0. (B) Change with time in the observed fractional yield of *d*-DHA (see eq 4): (●) reaction catalyzed by 0.30 mM XI at pD 7.0, (▲) reaction catalyzed by 0.27 mM XI at pD 7.0, and (□) reaction catalyzed by 0.20 mM XI at pD 8.0.

Steady State Kinetic Studies. Values of V_{max} and K_m for the XI-catalyzed isomerization of D-xylose to give D-xylulose in D_2O at pD 7.0 or 8.0 in the presence of 24 mM imidazole and 10 mM $MgCl_2$ at 25 °C and I = 0.10 (NaCl) were determined from the nonlinear least-squares fit of the initial velocity data to the Michaelis–Menten equation. The value of K_i for competitive inhibition of XI by DGA was determined from the nonlinear least-squares fit of the initial velocities, v, to eq 5. The quoted errors are standard deviations. The initial velocities determined in these experiments could be reproduced to better than ±5%.

$$\frac{v}{V_{max}} = \frac{[S]}{[S] + K_m\left(1 + \frac{[I]}{K_i}\right)} \quad (5)$$

RESULTS

Kinetic and Product Studies. D-Xylose isomerase from *S. rubiginosus* was assayed in D_2O by coupling the enzyme-catalyzed isomerization of D-xylose to form D-xylulose to the reduction of D-xylulose by NADH using sorbitol dehydrogenase. Table 1 reports the values of k_{cat} and K_m determined for the XI-catalyzed isomerization of D-xylose in D_2O at pD 7.0 in the presence of 24 mM imidazole buffer and 10 mM $MgCl_2$ at 25 °C and I = 0.1 (NaCl). A k_{cat} of 3.3 s^{-1} and a K_m of 5.0 mM at pD 8.0 were determined for this isomerization reaction under otherwise similar conditions. By comparison, the XI-catalyzed (*Streptomyces violaceoruber*) isomerization of D-xylose in H_2O at 35 °C exhibits a broad pH optimum at neutral pH, with a k_{cat} of 10 s^{-1} and a K_m of 2.8 mM.[23]

The inhibition of the XI-catalyzed isomerization of D-xylose by DGA at pD 7.0 was examined using six concentrations of D-xylose between 2.5 and 30 mM and fixed DGA concentrations of 3.2 and 6.3 mM (data not shown). The presence of DGA does not change the maximum velocity for the reaction in the presence of a saturating amount of D-xylose. This shows that

Table 1. Kinetic Parameters for Isomerization of D-Glyceraldehyde (DGA) and D-Xylose Catalyzed by D-Xylose Isomerase from *Streptomyces rubiginosus* in D_2O at 25 °C[a]

substrate	pathway	k_{cat} (s^{-1})	K_m (M)	k_{cat}/K_m (M^{-1} s^{-1})
DGA	total	1.0×10^{-4}	3×10^{-3}	0.034 (0.035)[b]
DGA[c]	hydride transfer	9×10^{-5}	3×10^{-3}	0.031
DGA[d]	proton transfer	1×10^{-5}	3×10^{-3}	3×10^{-3}
D-xylose	hydride transfer	2.4	4.9×10^{-3}	490

[a]At pD 7.0 in the presence of 24 mM imidazole buffer and 10 mM $MgCl_2$ at I = 0.1 (NaCl), unless noted otherwise. Rate constants are reported for the reaction of total DGA or D-xylose. [b]Data for the reaction at pD 8.0. [c]Kinetic parameters for the reaction with intramolecular transfer of hydrogen to form *h*-DHA, calculated from the observed kinetic parameters and the 90% fractional yield of *h*-DHA. [d]Kinetic parameters for the reaction with transfer of deuterium from solvent to product to form *d*-DHA, calculated from the observed kinetic parameters and the 10% fractional yield of *d*-DHA.

inhibition by DGA is competitive. An inhibition constant (K_i) for DGA of 3.0 ± 0.1 mM was determined from the nonlinear least-squares fit of the initial velocity data to eq 5. The initial velocities determined for the XI-catalyzed isomerization of 21 mM D-xylose in the presence of 5.3 and 10.3 mM DGA at pD 8.0 are also consistent with a K_i of 3 mM for DGA, which shows that there is no large change in K_i for the enzyme-catalyzed reaction upon moving to the higher pD.

The nonenzymatic reaction of DGA in D_2O at pD 7.0 in the presence of 24 mM imidazole buffer and 10 mM $MgCl_2$ at 25 °C and I = 0.1 (NaCl) was monitored by ^1H NMR for 3 weeks, during which time ~25% of the starting DGA disappeared. The major reaction products were formate and glycolaldehyde from the oxidative cleavage of DGA. There was no detectable formation of DHA from a nonenzymatic aldose–ketose isomerization reaction. These data gave a $(k_N)_{app}$ of ≈1.4×10^{-7} s^{-1} as the net observed rate constant for all of the nonenzymatic reactions of DGA (Scheme 3).

Scheme 3

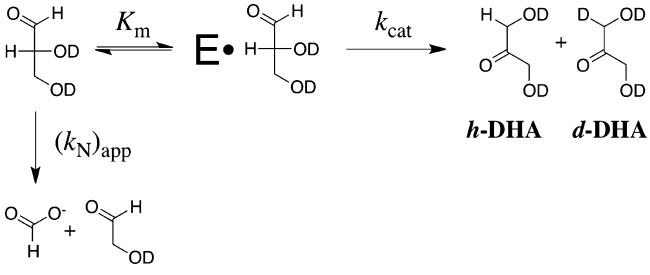

The XI-catalyzed isomerization of DGA in D_2O at pD 7.0 or 8.0 in the presence of 24 mM imidazole buffer and 10 mM $MgCl_2$ at 25 °C and I = 0.1 (NaCl) was monitored by ^1H NMR spectroscopy for ~9 h, during which time ~10% of the starting DGA disappeared. Figure 1A shows the linear initial rate time courses, with slope k_{obsd}, for the fractional conversion of 11 mM DGA to give *h*-DHA and *d*-DHA, $(f_{DHA})_{tot}$ (eq 1), catalyzed by XI at pD 7.0 ([E] = 0.30 mM) or pD 8.0 ([E] = 0.20 mM). Values of the apparent first-order rate constants (k_{obsd}), (2.2 ± 0.1) × 10^{-6} and 1.5 × 10^{-6} s^{-1} at pD 7.0 and 8.0, respectively, were determined from the slopes of the linear correlations in Figure 1A (eq 2), where the quoted error is the standard deviation in this slope. The values of k_{cat} and k_{cat}/K_m

dx.doi.org/10.1021/bi201378c | *Biochemistry* 2011, 50, 10170–10181

(Table 1) for the XI-catalyzed isomerization of DGA in D_2O (Scheme 3) were obtained from the apparent first-order rate constants using eq 6, with the assumption that the K_i of 3 mM determined for competitive inhibition by DGA of the XI-catalyzed reaction of D-xylose is equal to the K_m for the XI-catalyzed reaction of DGA.

$$k_{obsd} = \frac{k_{cat}[E]}{K_m + [DGA]_0} \quad (6)$$

Figure 2 shows representative partial ^1H NMR spectra of in the region of the free keto form of DHA, obtained during the

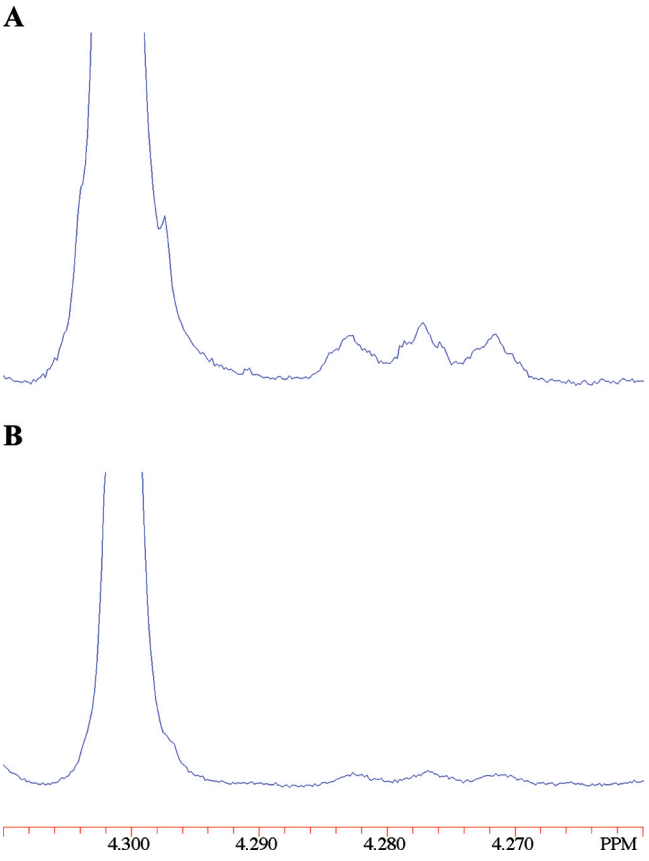

Figure 2. Representative partial ^1H NMR spectra at 500 MHz obtained during the XI-catalyzed isomerization reaction of 11 mM DGA in D_2O in the presence of 24 mM imidazole buffer and 10 mM $MgCl_2$ at 25 °C and I = 0.1 (NaCl). The large singlet at 4.300 ppm is the signal for the two α-CH_2OD groups of *h*-DHA and the single α-CH_2OD group of *d*-DHA. The upfield-shifted triplet at 4.276 ppm is the signal for the single α-CHDOD group of *d*-DHA. (A) Reaction catalyzed by 0.30 mM XI at pD 7.0. The area of the triplet is 2.5% of that of the singlet. (B) Reaction catalyzed by 0.20 mM XI at pD 8.0. The area of the triplet is 1.2% of that of the singlet.

XI-catalyzed isomerization of DGA in D_2O. The singlet at 4.300 ppm with an area A_{CH2} is due to the α-CH_2OD groups of both *h*-DHA and *d*-DHA, and the 0.024 ppm upfield-shifted triplet with an area A_{CHD} is due to the α-CHDOD group of *d*-DHA (Scheme 3). In these spectra, the area A_{CHD} is ~2.5 and ~1.2% of that of the area A_{CH2} for reactions at pD 7.0 (Figure 2A) and pD 8.0 (Figure 2B), respectively. Figure 1B shows the change with time in the fraction of the product DHA that is labeled with deuterium at pD 7.0 and 8.0, determined from the peak areas A_{CH2} and A_{CHD} using eqs 3 and 4. The increase in $f_{d\text{-DHA}}/(f_{DHA})_{tot}$ with time results from the slow XI-catalyzed deuterium exchange of the methylene protons of the product *h*-DHA to give additional *d*-DHA. The initial fractions of the product DHA that contains deuterium, 0.095 and 0.05 at pD 7.0 and 8.0, respectively, were estimated by making a short linear extrapolation of the data in Figure 1B to zero reaction time. Table 1 reports the values of k_{cat}/K_m for the XI-catalyzed isomerization of DGA with intramolecular hydride transfer to give *h*-DHA and with proton transfer with incorporation of deuterium from solvent D_2O to give *d*-DHA, calculated from the kinetic parameters for the overall XI-catalyzed isomerization of DGA and these fractional product yields.

No products of XI-catalyzed isomerization were detected during the reaction of 11 mM DGA for 9 h in D_2O at pD 7.0 in the presence of 24 mM imidazole buffer, 10 mM $MgCl_2$, 0.27 mM XI, and the competitive inhibitor D-threonohydroxamic acid at 0.5 mM ($5000K_i$)[28] at 25 °C and I = 0.1 (NaCl).

The XI-catalyzed isomerization of DHA (11 mM) in D_2O at pD 7.0 in the presence of 24 mM imidazole buffer and 10 mM $MgCl_2$ and 0.30 mM XI at 25 °C and I = 0.1 (NaCl) was monitored by ^1H NMR spectroscopy for ~25 h, during which time ~6% of the starting *h*-DHA had undergone deuterium exchange with solvent to form *d*-DHA. Small amounts of *h*-DGA and *d*-DGA (~3% of total DHA) from thermodynamically unfavorable isomerization were also detected. No products of the enzyme-catalyzed deuterium exchange or isomerization reactions of DHA were detected by ^1H NMR after a 25 h reaction time under the same conditions, but in the presence of 0.5 mM D-threonohydroxamic acid.

X-ray Crystallographic Analyses. XI crystallized in space group *I*222 with the following unit cell dimensions: a = 92.6 Å, b = 98.1 Å, and c = 102.6 Å. XI from *Streptomyces olivochromogenes* has been shown to crystallize in space group $P2_12_12$ with pseudo-*I*222 symmetry.[15] However, these data were not collected from crystals cooled to 100 K. The first XI structure determined from cryogenic data displayed true *I*222 symmetry.[16] Given that attempts to refine these structures in several orthorhombic space groups failed, we conclude that *I*222 is also the true space group for these crystals. Data collection and refinement statistics for the structures of XI crystals obtained after they had been soaked for 9 h in a solution that contained 50 mM DGA are presented in Table 2. The structure at 0.97 Å resolution (Figure 3) showed electron density that was modeled as two ligands bound at the enzyme active site: the hydrate of DGA (DGAH, 49% occupancy) and formate ion (51% occupancy). The C-3 hydroxyl of DGAH interacts with the protein through a hydrogen bond to N-ε of the imidazole side chain of His54 (2.6 Å) and to a bridging water molecule, with the γ-oxygen of Thr90 (2.8 Å). XI shows good catalytic activity with either Mg^{2+} or Mn^{2+} bound at the two metal sites.[22] We have worked with the Mg^{2+} enzyme. The C-2 hydroxyl is coordinated to M-1 (2.1 Å). The two C-1 hydroxyls of DGAH, O-a and O-b, interact with M-1 (2.2 Å) and with an ordered solvent molecule. One oxygen atom of formate ion is found to bridge M-1 and M-2a (2.2 and 2.5 Å, respectively). The second oxygen is coordinated to M-2a (2.3 Å) and interacts by hydrogen bonding with the ζ-ammonium ion of Lys183 (3.1 Å). The water/hydroxide ion ligand of M-2a is 2.0 Å from the Mg^{2+} atom. In this arrangement, the binding of DGAH and formate appears to be mutually exclusive. A second structure (not shown) of XI soaked with DGA for a period of 15 min is nearly identical to the structure of DGAH despite the much shorter soaking time.

Table 2. Statistics from X-ray Data Collection and Refinement

Data Collection Statistics	
resolution (Å) (last shell)[a]	20.00−0.97 (1.00−0.97)
wavelength (Å)	0.9399
no. of reflections	
observed	7151163
unique	272713
completeness (%)[a]	99.7 (96.7)
R_{merge} (%)[a,b]	5.5 (39.4)
redundancy	8.5 (5.4)
$I/\sigma(I)$[a]	39.5 (3.4)
Refinement Statistics	
no. of reflections in the working set	262140
no. of reflections in the test set	13001
R_{cryst} (R_{free})	0.116 (0.125)
no. of non-hydrogen atoms	3206
no. of solvent atoms	523
average B factor (Å^2)	
protein atoms	11.0
DGAH/FMT	8.2/8.4
Mg(II) ions	8.6
solvent	25.1
root-mean-square deviation	
bond lengths (Å)	0.008
bond angles (deg)	1.343

[a]Data for the highest-resolution shell are given in parentheses. [b]$R_{merge} = \sum_{hkl}\sum_i |I_{hkl,i} - \langle I_{hkl}\rangle I| / \sum_{hkl}\sum_i |I_{hkl,i}|$, where $\langle I_{hkl}\rangle$ is the mean intensity of the multiple $I_{hkl,i}$ observations for symmetry-related reflections.

DISCUSSION

There are two pathways for the slow TIM-catalyzed reactions of the neutral truncated substrates DGA and glycolaldehyde in D_2O: (1) a reaction at the enzyme active site that is stopped by binding of the competitive inhibitor 2-phosphoglycolate (PGA) and (2) a reaction that is insensitive to PGA and/or to mutations that cripple the reaction of the natural substrate DGAP at the enzyme active site.[8] This second nonspecific reaction pathway has also been documented for the reaction of glycolaldehyde catalyzed by bovine serum albumin.[39] By contrast, the observed XI-catalyzed isomerization of DGA to give DHA is completely abolished by the tight-binding competitive inhibitor D-threonohydroxamic acid,[28] which shows that this isomerization occurs exclusively at the enzyme active site. Similarly, the very slow XI-catalyzed deuterium exchange reaction of DHA is also completely inhibited by the binding of D-threonohydroxamic acid.

XI-Catalyzed Isomerization of DGA. The XI-catalyzed isomerization of [2-^{3}H]-D-glucose in water at pH 7 proceeds with transfer of tritium from substrate to solvent approximately once every 10^9 substrate turnovers to form product.[13] This is consistent with intramolecular hydride transfer in conversion of the α-hydroxy aldehyde to the α-hydroxy ketone, and a very rare competing enzyme-catalyzed proton transfer reaction. The improbable alternative proton transfer mechanism would require an extraordinary level of shielding of a putative catalytic side chain that shuttles the proton between the two reacting carbon atoms.[13] By contrast, the XI-catalyzed isomerization of DGA to give DHA in D_2O reported here proceeds with incorporation of 0.10 and 0.05 mole fraction of deuterium for the reactions at pD 7.0 and 8.0, respectively (Figure 1B), so that at least 5−10% of the reaction of the truncated substrate proceeds by a proton transfer mechanism (Scheme 4). We also find that XI catalyzes the slow transfer of deuterium from solvent D_2O into DHA to give *d*-DHA [k_{ex} (Scheme 4)]. The XI-catalyzed reactions of both DGA and DHA are abolished by the binding of the competitive inhibitor D-threonohydroxamic acid.[28]

We conclude that turnover of the minimal substrate DGA by XI proceeds by the competing hydride and proton transfer pathways (Scheme 4) previously observed for the nonenzymatic isomerization of DGA in aqueous solution.[19,20] Therefore, the interaction between the terminal CH(OH)-CH_2OH fragment of D-xylose and XI appears to provide a specific stabilization of the transition state for enzyme-catalyzed isomerization with intramolecular hydride transfer, so that the truncation of this fragment results in a large increase in the relative rate of the reaction with proton transfer. We suggest that the very rare tritium exchange reaction of [2-^{3}H]-D-glucose and the isomerization of DGA with transfer of deuterium from solvent to product DHA catalyzed by XI proceed by adventitious deprotonation of bound substrate by a basic residue at the enzyme active site. There is ample precedent for nonspecific protein-catalyzed deprotonation of α-carbonyl carbon with second-order rate constants similar to that reported here for XI. The k_{cat}/K_m value of 3×10^{-3} M^{-1} s^{-1} for the XI-catalyzed isomerization of DGA by proton transfer to give *d*-DHA (Table 1) is 10-fold larger than the k_N of 3.2×10^{-4} M^{-1} s^{-1} for nonenzymatic deprotonation of DGA by the tertiary amine 3-quinuclidinone (Table 3),[26] but it is similar to the k_{cat}/K_m values of 0.013 and 3×10^{-3} M^{-1} s^{-1} determined for the deuterium exchange reactions of glycolaldehyde in D_2O catalyzed by bovine serum albumin and the crippled K12G mutant of yeast TIM, respectively.[8,39]

There is a decrease in the fractional yield of *d*-DHA from the XI-catalyzed isomerization of DGA in D_2O from 9.5 to 5% upon moving from pD 7.0 to 8.0 (Figure 1B), but this increase in pD results in no significant change in the value of k_{cat}/K_m for the overall reaction that gives *h*-DHA as the major product (Table 1). Therefore, the rate-determining step for the overall isomerization reaction is pD-independent in this range, but the dependencies on pD of the steps that determine the relative yields of *h*-DHA and *d*-DHA are different. We are unable to provide a simple explanation for these data.

DGA is a competitive inhibitor of the XI-catalyzed isomerization of D-xylose in D_2O with a K_i of 3.0 mM that is similar to the K_m of 4.9 mM for isomerization of D-xylose under the same conditions (Table 1). Therefore, the addition of an ethylene glycol fragment to DGA to give D-xylose does not change the apparent stability of the complex with XI. The observation that the addition of this fragment to DGA results in a large increase in k_{cat}/K_m for XI-catalyzed isomerization by hydride transfer from 0.034 to 490 M^{-1} s^{-1} (Table 1) shows that its interactions with XI are expressed only in the transition state and are therefore utilized to stabilize the linear sugar in the transition state relative to the cyclic sugar in the Michaelis complex.

The data in Table 3 show that at pD 7.0 TIM provides an only 50-fold rate acceleration of the reference nonenzymatic deprotonation of DGA by the small Brønsted base catalyst 3-quinuclidinone in D_2O,[26] while XI provides a somewhat larger 2100-fold rate acceleration of the reference nonenzymatic Zn^{2+}-catalyzed isomerization reaction of DGA that is promoted by

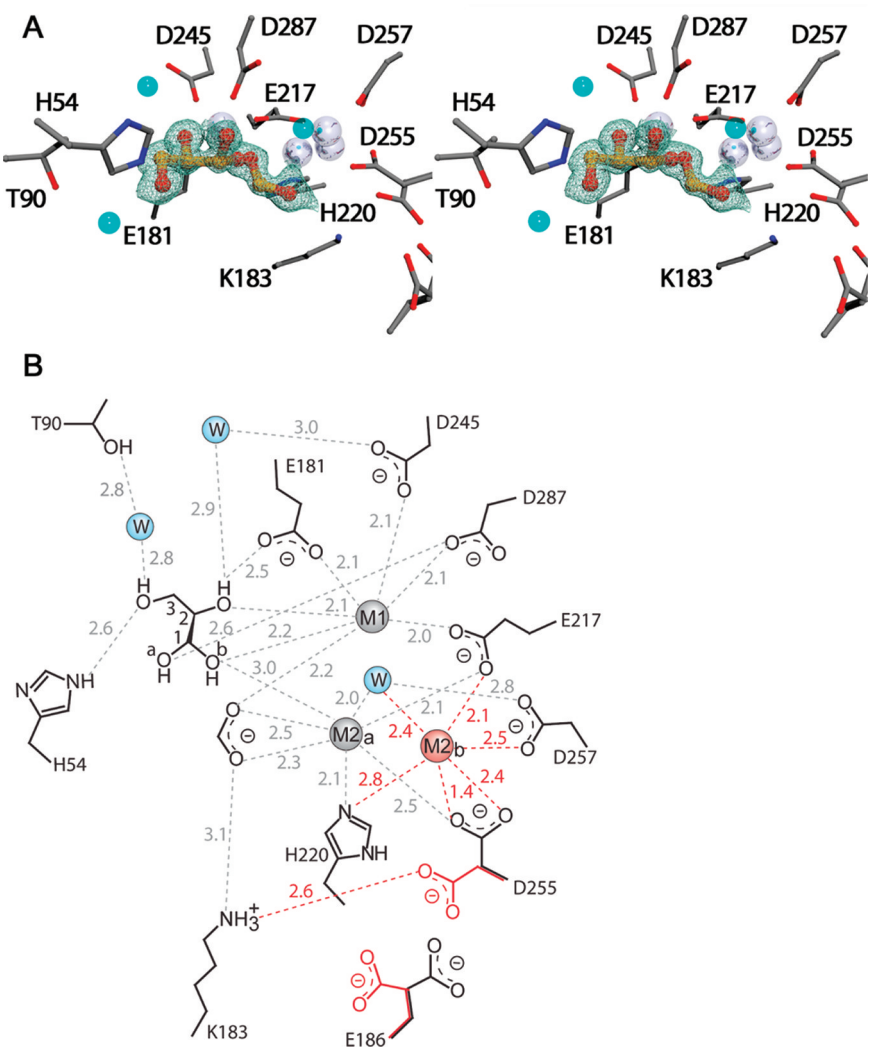

Figure 3. Structure of the XI active site complexed with DGAH. (A) Shown as a stereoview with the $|F_o| - |F_c|$ simulated annealing omit electron density map shown as a light blue wireframe, the metal ions as silver spheres, and the water molecules as blue spheres. These figures were generated with the POVSCRIPT+ modification of MOLSCRIPT[60] and POV-Ray[61] (http://www.povray.org/). (B) Diagram of the structure that shows the waters as blue spheres and the hydrogen bonds as dashed lines labeled with distances in angstroms. The atoms and corresponding distances in red indicate those with partial occupancy.

Scheme 4

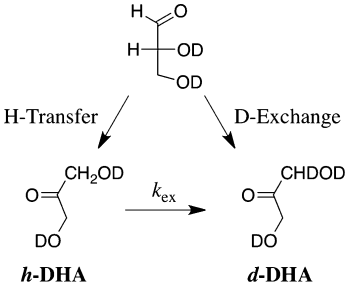

lyoxide ion shown in Scheme 5.[20] The similar observed catalytic activities of XI (k_{cat}/K_m = 0.034 M^{-1} s^1) and TIM (k_{cat}/K_m = 0.017 M^{-1} s^{-1}) toward isomerization of the common minimal substrate DGA by hydride transfer and proton transfer, respectively (Table 3), therefore require that the difference in the kinetic parameters for catalysis of the isomerization of the whole substrates D-xylose and DGAP, respectively, by these enzymes result from different contributions of the intrinsic binding energy of the nonreacting portions of the substrate to stabilization of the transition state.[40]

Insights from Crystallography. TIM shows a strong selectivity for the binding and reaction of the reactive carbonyl form of DGAP.[27] This probably reflects the snug fit of ligands at the active loop-closed enzyme[41,42] and the exclusion of the sterically demanding hydrated substrate. By contrast, we report here that the X-ray crystal structure of the complex obtained by soaking XI in a solution that contains 50 mM total DGA shows that the ligand is bound as DGA hydrate [DGAH (Figure 3)]. Because XI forms an initial Michaelis complex with the cyclic form of glucose/xylose,[14,43,44] there is no obvious requirement that the enzyme show selectivity toward binding the carbonyl form of the truncated substrate DGA. It would appear that this selectivity for the reactive carbonyl form of the substrate is provided by the subsequent development of strong interactions of the enzyme with the C-4 and C-5 hydroxyls of the linear form of the full substrate D-xylose in the transition state (see below). While the binding mode observed herein for the DGAH·formate complex is strikingly similar to that of the cyclic form of glucose [PDB entry 1XIF (Figure 4A)], it is a closer

dx.doi.org/10.1021/bi201378c|*Biochemistry* 2011, 50, 10170–10181

Table 3. Enzymatic Rate Accelerations for Turnover of the Whole Substrates and the Common Substrate Fragment D-Glyceraldehyde by D-Xylose Isomerase and Triosephosphate Isomerase

catalyst	substrate	pathway	k_N[a] (M^{-1} s^{-1})	k_{cat}/K_m (M^{-1} s^{-1})	rate effect[b]	fragment binding energy (kcal/mol)
Zn^{2+}	DGA	hydride transfer	1.6×10^{-5}[c]			
Zn^{2+}	D-xylose		3.2×10^{-8}[d]			
XI	DGA			0.034[e]	2100	9.3[f]
XI	D-xylose			490[e]	1.5×10^{10}	
buffer[g]	DGA	proton transfer	3.2×10^{-4}[h]			
TIM	DGA			0.017[h]	50	11.9[j]
TIM	DGAP			9.6×10^{6}[i]	3×10^{10}	

[a]Second-order rate constants for the reference nonenzymatic isomerization reactions of total DGA or D-xylose in D_2O at pD 7.0 and 25 °C. [b]The enzymatic rate acceleration calculated as the ratio of the second-order rate constants for the enzyme-catalyzed reaction and the reference nonenzymatic reaction catalyzed by Zn^{2+} or the Brønsted base 3-quinuclidinone in aqueous solution. [c]Calculated as $k_{Zn} = k_T[DO^-]$, where k_T = 950 M^{-2} s^{-1} is the third-order rate constant for the lyoxide ion-promoted Zn^{2+}-catalyzed isomerization of total DGA and $[DO^-] = 1.7 \times 10^{-8}$ M at pD 7.0 (data from ref 20). [d]Calculated from k_{Zn} for isomerization of DGA with a 500-fold correction for the fraction of D-xylose that is smaller than that of DGA present in the reactive carbonyl form. We make the assumption that the free carbonyl forms of DGA and D-xylose have similar reactivities in the Zn^{2+}-catalyzed isomerization by hydride transfer (see the text). [e]Data at pD 7.0 from Table 1. [f]The intrinsic binding energy of the terminal $CH(OH)CH_2OH$ fragment of D-xylose, calculated from the ratio of the enzymatic rate accelerations for the XI-catalyzed reactions of D-xylose and DGA. [g]Data for nonenzymatic deprotonation of DGA by the tertiary amine base 3-quinuclidinone. We make the assumption that DGA and DGAP have similar reactivities in nonenzymatic proton transfer. [h]Data from ref 26. [i]Calculated from a k_{cat} of 4300 s^{-1} and a K_m of 0.45 mM for turnover of total DGAP by rabbit muscle TIM in H_2O at pH 7.5 and 25 °C.[26] [j]The intrinsic binding energy of the phosphodianion group of DGA, calculated from the ratio of the enzymatic rate accelerations for the TIM-catalyzed reactions of DGAP and DGA.

Scheme 5

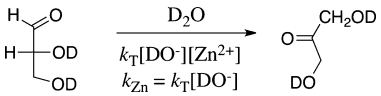

match to that of the linear xylulose [PDB entry 1XII (Figure 4B)]. Because these small fragments can adopt multiple binding orientations in the active site, this finding highlights a preference of XI for binding the linear forms of pentose/hexose sugars.

The structure of XI with bound hydrated triose does not represent a productive complex because of both the presence of the hydrate form and the orientation of C-1/C-2 with respect to the catalytic metals (the C-2 hydroxyl group does not bridge M-1 and M-2 as expected for the hydride transfer mechanism). However, the DGAH structure does show that binding of the triose substrate can induce conformational changes in active site residues that are remarkably similar to those observed in structures with bound pentose and hexose substrates (Figure 4). Specifically, the X-ray structures demonstrate that in addition

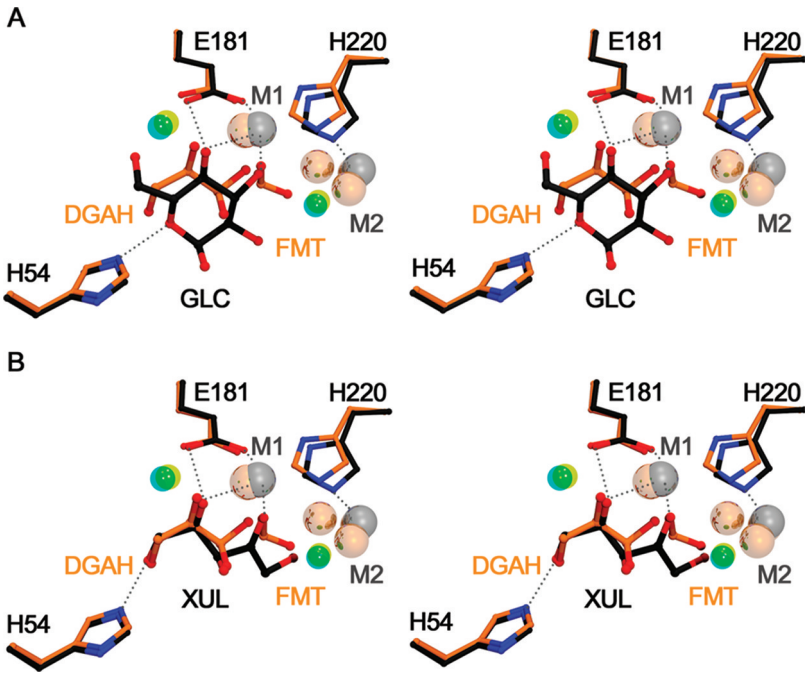

Figure 4. Overlays of the structure of XI complexed with DGAH, formate, and Mg^{2+} (DGHA and FMT with a yellow backbone, Mg^{2+} as light gray spheres, H_2O as cyan spheres) with those of (A) the cyclic form of D-glucose (GLC with a gray backbone, Mg^{2+} as dark gray spheres, H_2O as a yellow sphere, PDB entry 1XIF) and (B) the linear form of D-xylulose (XUL with a gray backbone, Mg^{2+} as dark gray spheres, H_2O as a yellow sphere, PDB entry 1XII). The hydrogen and coordination bonds are shown for the D-glucose and D-xylose ligands as gray dashed lines. Models were superimposed with the SSM algorithm as implemented in COOT. This figure was prepared using MOLSCRIPT.[60]

dx.doi.org/10.1021/bi201378c | Biochemistry 2011, 50, 10170–10181

to the mobility of the M-2 metal center, the catalytic residues Glu181, Glu186, Asp255, and Asp257 adopt alternate conformations upon substrate binding compared to those observed in unliganded XI. This finding is also consistent with EPR spectroscopy studies on XI that show that binding of the cyclic form of substrates or substrate analogue inhibitors is sufficient to induce the shift of the metal ion in this site.[45] A recent joint X-ray and neutron diffraction study shows that the catalytic metal, M-2, occupies two sites after ring opening and before isomerization.[46] Thus, the metal ion movement may well be independent and not necessarily coupled to the isomerization reaction hypothesized to take place from the linear form of the sugar.

Rate Acceleration and Intrinsic Binding Energies for XI-Catalyzed Isomerization. The linear open form of D-xylose and the free carbonyl form of DGA are expected to show a similar intrinsic chemical reactivity in nonenzymatic Zn^{2+}-catalyzed isomerization by hydride transfer in aqueous solution. However, the apparent rate constant for Zn^{2+}-catalyzed isomerization of D-xylose should be ~500-fold smaller than the observed rate constant for isomerization of DGA at the same pD (Scheme 5). This is because the fraction of D-xylose present as the reactive linear sugar [0.01% (Scheme 6)[47]] is

Scheme 6

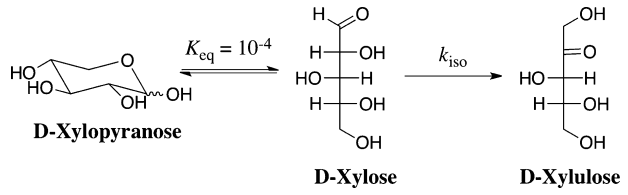

500-fold smaller than the fraction of DGA present as the reactive free aldehyde (5%[26]). A 500-fold correction of the apparent second-order rate constant for nonenzymatic Zn^{2+}-catalyzed isomerization of DGA by hydride transfer at pD 7.0 [$k_{Zn} = k_T[DO^-] = 1.6 \times 10^{-5}$ M^{-1} s^{-1} (Scheme 5)] gives an estimated rate constant (k_{Zn}) of 3.2×10^{-8} M^{-1} s^{-1} for the Zn^{2+}-catalyzed isomerization of D-xylose under the same conditions (Table 3). This can then be combined with a k_{cat}/K_m of 490 M^{-1} s^{-1} for the XI-catalyzed isomerization of D-xylose to give an estimated enzymatic rate acceleration for isomerization of D-xylose of 1.5×10^{10}-fold (Table 3).

The data for the XI-catalyzed reaction of DGA allow us to portion the 1.5×10^{10}-fold rate acceleration for the XI-catalyzed isomerization of D-xylose into a smaller 2100-fold rate acceleration for reaction of the truncated substrate DGA (Table 3) and a much larger 7×10^6-fold rate acceleration that is due to specific stabilization of the transition state for isomerization by interactions between XI and the terminal ethylene glycol fragment of D-xylose. This corresponds to an apparent 9.3 kcal/mol intrinsic binding energy for this substrate fragment. By comparison, a larger ~12 kcal/mol intrinsic binding energy is estimated for the nonreacting substrate phosphodianion group in the TIM-catalyzed isomerization of DGAP.[26,48] The larger phosphodianion binding energy underscores the greater strength of electrostatic interactions between fully charged species, such as between the phosphodianion of DGAP and the alkylammonium side chain of Lys12 at TIM,[8,49] compared with interactions with neutral hydrogen bond donors and acceptors.

The 9.3 kcal/mol intrinsic binding energy of the terminal ethylene glycol fragment of D-xylose is similar to that observed for other enzymatic reactions of sugars. For example, intrinsic transition state binding energies of 4−6 kcal/mol per sugar hydroxyl group have been reported for enzyme-catalyzed glycosyl transfer reactions.[50] An unusually large 10 kcal/mol intrinsic binding energy was reported for the galactosyl C-2 hydroxyl in the breakdown of the covalent β-D-galactopyranosyl intermediate of β-galactosidase-catalyzed glycosyl transfer reactions.[51]

The structure of XI determined by the time-of-flight neutron Laue method has been used to identify the location of the hydrogen atoms of enzyme-bound D-xylulose.[52,53] The neutron diffraction and X-ray crystal structures[15,16,25,54] of XI show that the C-4 hydroxyl of the substrate interacts with the metal ion designated as M-1, and that the C-5 hydroxyl is hydrogen bonded to N-ε2 of His54. The neutron diffraction structure requires a surprising perturbation in the relative pK_a values for the C-5 sugar hydroxyl and N-ε2 of His54 that results in formal proton transfer from the substrate oxygen to the protein imidazole. This suggests that the complex of the O-ionized sugar is stabilized by a strong, single-potential minimum hydrogen bond[55,56] to the cationic N-ε2 of His54.[53]

Ground State and Transition State Effects. The K_m value of 4.9 mM for the XI-catalyzed isomerization of D-xylose at pD 7.0 is not significantly different from the K_m that approximates the K_i of 3.0 mM for DGA (Table 1). This shows that the binding interactions between XI and the terminal ethylene glycol fragment of D-xylose are not expressed in the Michaelis complex with D-xylose. Rather, these interactions develop on proceeding from the Michaelis complex between XI and the cyclic sugar to the transition state for sugar isomerization and are expressed in the much larger k_{cat} value of 2.4 s^{-1} for D-xylose compared with the k_{cat} of 9.0×10^{-5} s^{-1} for XI-catalyzed isomerization of DGA by hydride transfer (Table 1).

There is a normal primary kinetic deuterium isotope effect on the XI-catalyzed isomerization of [2-^{2}H]-D-glucose that shows that the ring opening of glucose is a fast and reversible step that precedes rate-determining intramolecular hydride transfer.[57,58] A simple explanation for the observed effects of substituents on k_{cat} and K_m is that the interactions between XI and the C-4 hydroxyl and the C-5 ring oxygen of D-xylose are minimal in the ground state Michaelis complex with the cyclic sugar and develop only after ring opening of D-xylose to form the linear sugar. This must be the case for the hydrogen bond between the C-5 hydroxyl of the linear sugar and the cationic N-ε2 of His54.[53] We propose that the interaction between the C-4 hydroxyl of D-xylose and the metal ion designated as M-1 is also weak or absent in the productive complex with the cyclic sugar. If the interactions between XI and the C-4 and C-5 hydroxyl develop only upon conversion of cyclic D-xylose to the linear form, then the affinity of the linear sugar for XI will be much higher than that of the cyclic form of D-xylose. In fact, linear D-xylitol typically shows a higher affinity for XI than D-xylose does.[22,59] For example, the K_i of 0.026 mM for inhibition of XI-catalyzed [*Streptomyces* sp. (ATCC 21132)] isomerization by xylitol at pH 7.1 is more than 100-fold smaller than the K_m of 3.1 mM for the isomerization of D-xylose.[22]

XI and TIM use different strategies to obtain an increase in k_{cat} through the utilization of enzyme−ligand binding interactions to obtain specific transition state stabilization relative to the Michaelis complex. In the case of XI, the substrate ring opening is a step on the pathway from the Michaelis complex to the transition state, and the new binding

interactions that develop with the open linear sugar are expressed as an increase in k_{cat}. There is good evidence that a tightening of the electrostatic interactions between the cationic side chain of Lys12 and the bound substrate DGAP on proceeding from the Michaelis complex (substrate dianion) to the transition state (enediolate-like trianion) result in an ~10^5-fold increase in k_{cat} for TIM-catalyzed isomerization.[8]

SUMMARY AND CONCLUSIONS

XI achieves its catalytic power through the summation of several stabilizing interactions between the protein catalyst and the substrate pieces. The enzyme provides a 2100-fold increase in the second-order rate constant for metal ion-catalyzed isomerization by hydride transfer in D_2O. The K_m of 3 mM for the XI-catalyzed isomerization of DGA is consistent with a modest stabilization of the Michaelis complex. However, the X-ray crystal structure of this complex shows the triose bound as the unreactive hydrate (DGAH). If the dominant XI·DGAH complex is nonproductive, then the binding of DGA as the productive Michaelis complex must be relatively weak and the weak binding compensated by effective protein activation of catalysis by the metal cation. The transition state for aldose–ketose isomerization of D-xylose is stabilized by 9.3 kcal/mol by interactions of XI with the C-4 and C-5 hydroxyls of the substrate. This significant, but not extraordinarily strong, interaction can be rationalized by an examination of the neutron diffraction[52,53] and X-ray crystal structures[15,16,25,54] of XI·sugar complexes. The larger kinetic parameters for catalysis by TIM compared with those of XI are due to (i) the smaller catalytic burden borne by TIM, which must overcome an only 1.7 kcal/mol barrier to dehydration of DGAP to give the free carbonyl form, compared with that borne by XI, which must overcome a 5.4 kcal/mol barrier for ring opening of D-xylose, and (ii) the larger ~12 kcal/mol intrinsic binding energy for the phosphodianion fragment of DGAP, compared with the 9.3 kcal/mol binding energy of the terminal ethylene glycol fragment of D-xylose (Table 3).

The major impediment to perfection in enzymatic catalysis of isomerization of D-xylose is the evolution of an enzyme active site capable of accommodating the very different structures of the cyclic (99.99%) and linear (0.01%) forms of D-xylose.[47] The higher affinity of XI for linear xylitol than for the cyclic sugars suggests that this catalyst has evolved to optimize binding interactions with linear sugars, while the large K_m of 4.9 mM for D-xylose in D_2O (Table 1) shows that cyclic sugars bind relatively weakly. It is interesting that the apparent k_{cat}/K_m of 490 M^{-1} s^{-1} for XI-catalyzed isomerization of D-xylose in D_2O (Table 1) and the fraction of sugar present in the linear form (10^{-4}) are consistent with a k_{cat}/K_m value of 4.9×10^6 M^{-1} s^{-1} for direct catalysis of the isomerization of linear D-xylose. This rate constant is not far removed from that for a diffusion-controlled reaction, such as that conducted by TIM.

ASSOCIATED CONTENT

Accession Codes

The coordinates of the refined structure have been deposited with the Protein Data Bank as entry 3U3H.

AUTHOR INFORMATION

Corresponding Author

*Telephone: (716) 645-4232. Fax: (716) 645-6963. E-mail: jrichard@buffalo.edu.

Funding

This work was supported by Grant GM 39754 from the National Institutes of Health.

ABBREVIATIONS

DGA, D-glyceraldehyde; *h*-DGA, [1(*R*)-^{1}H]glyceraldehyde; *d*-DGA, [2(*R*)-^{2}H]glyceraldehyde; DGAH, hydrate of D-glyceraldehyde; DGAP, (*R*)-glyceraldehyde 3-phosphate; DHA, dihydroxyacetone; *h*-DHA, [1-^{1}H]dihydroxyacetone; *d*-DHA, [1-^{2}H]dihydroxyacetone; NADH, nicotinamide adenine dinucleotide, reduced form; NMR, nuclear magnetic resonance; PGA, 2-phosphoglycolate; TIM, triosephosphate isomerase; XI, D-xylose isomerase.

ADDITIONAL NOTE

[a]The rate constants for DGA and DGAP reported in the introductory section are calculated for the reaction of the minor (5%) free carbonyl form of the substrates. They are 20-fold larger than the corresponding observed rate constants that refer to the reaction of total DGA or DGAP given in Tables 1 and 3.

REFERENCES

(1) Knowles, J. R. (1991) Enzyme catalysis: Not different, just better. *Nature 350*, 121–124.

(2) Knowles, J. R. (1991) To build an enzyme. *Philos. Trans. R. Soc. London, Ser. B 332*, 115–121.

(3) Knowles, J. R., and Albery, W. J. (1977) Perfection in enzyme catalysis: The energetics of triosephosphate isomerase. *Acc. Chem. Res. 10*, 105–111.

(4) Malabanan, M. M., Amyes, T. L., and Richard, J. P. (2010) A role for flexible loops in enzyme catalysis. *Curr. Opin. Struct. Biol. 20*, 702–710.

(5) Rieder, S. V., and Rose, I. A. (1959) Mechanism of the triose phosphate isomerase reaction. *J. Biol. Chem. 234*, 1007–1010.

(6) Amyes, T. L., and Richard, J. P. (2007) Enzymatic catalysis of proton transfer at carbon: Activation of triosephosphate isomerase by phosphite dianion. *Biochemistry 46*, 5841–5854.

(7) Go, M. K., Amyes, T. L., and Richard, J. P. (2009) Hydron Transfer Catalyzed by Triosephosphate Isomerase. Products of the Direct and Phosphite-Activated Isomerization of [1-^{13}C]-Glycolaldehyde in D_2O. *Biochemistry 48*, 5769–5778.

(8) Go, M. K., Koudelka, A., Amyes, T. L., and Richard, J. P. (2010) Role of Lys-12 in Catalysis by Triosephosphate Isomerase: A Two-Part Substrate Approach. *Biochemistry 49*, 5377–5389.

(9) Lodi, P. J., and Knowles, J. R. (1991) Neutral imidazole is the electrophile in the reaction catalyzed by triosephosphate isomerase: Structural origins and catalytic implications. *Biochemistry 30*, 6948–6956.

(10) Farber, G. K., Petsko, G. A., and Ringe, D. (1987) The 3.0 Å crystal structure of xylose isomerase from *Streptomyces olivochromogenes*. *Protein Eng. 1*, 459–466.

(11) Farber, G. K., Machin, P., Almo, S. C., Petsko, G. A., and Hajdu, J. (1988) X-ray Laue diffraction from crystals of xylose isomerase. *Proc. Natl. Acad. Sci. U.S.A. 85*, 112–115.

(12) Glasfeld, A., Farber, G. K., Ringe, D., Marcel, T., Drocourt, D., Tiraby, G., and Petsko, G. A. (1988) Characterization of crystals of xylose isomerase from *Streptomyces violaceoniger*. *J. Biol. Chem. 263*, 14612–14613.

(13) Allen, K. N., Lavie, A., Farber, G. K., Glasfeld, A., Petsko, G. A., and Ringe, D. (1994) Isotopic Exchange plus Substrate and Inhibition Kinetics of D-Xylose Isomerase Do Not Support a Proton-Transfer Mechanism. *Biochemistry 33*, 1481–1487.

(14) Allen, K. N., Lavie, A., Glasfeld, A., Tanada, T. N., Gerrity, D. P., Carlson, S. C., Farber, G. K., Petsko, G. A., and Ringe, D. (1994) Role of the Divalent Metal Ion in Sugar Binding, Ring Opening, and

Isomerization by D-Xylose Isomerase: Replacement of a Catalytic Metal by an Amino Acid. *Biochemistry 33*, 1488−1494.
(15) Lavie, A., Allen, K. N., Petsko, G. A., and Ringe, D. (1994) X-ray Crystallographic Structures of D-Xylose Isomerase-Substrate Complexes Position the Substrate and Provide Evidence for Metal Movement during Catalysis. *Biochemistry 33*, 5469−5480.
(16) Fenn, T. D., Ringe, D., and Petsko, G. A. (2004) Xylose Isomerase in Substrate and Inhibitor Michaelis States: Atomic Resolution Studies of a Metal-Mediated Hydride Shift. *Biochemistry 43*, 6464−6474.
(17) Richard, J. P., and Amyes, T. L. (2001) Proton transfer at carbon. *Curr. Opin. Chem. Biol. 5*, 626−633.
(18) Richard, J. P. (1984) Acid-base catalysis of the elimination and isomerization reactions of triose phosphates. *J. Am. Chem. Soc. 106*, 4926−4936.
(19) Nagorski, R. W., and Richard, J. P. (1996) Mechanistic Imperatives for Enzymatic Catalysis of Aldose-Ketose Isomerization: Isomerization of Glyceraldehyde in Weakly Alkaline Solution Occurs with Intramolecular Transfer of a Hydride Ion. *J. Am. Chem. Soc. 118*, 7432−7433.
(20) Nagorski, R. W., and Richard, J. P. (2001) Mechanistic Imperatives for Aldose-Ketose Isomerization in Water: Specific, General Base- and Metal Ion-Catalyzed Isomerization of Glyceraldehyde with Proton and Hydride Transfer. *J. Am. Chem. Soc. 123*, 794−802.
(21) Blacklow, S. C., Raines, R. T., Lim, W. A., Zamore, P. D., and Knowles, J. R. (1988) Triosephosphate isomerase catalysis is diffusion controlled. *Biochemistry 27*, 1158−1165.
(22) Van Bastelaere, P., Vangrysperre, W., and Kersters-Hilderson, H. (1991) Kinetic studies of magnesium^{2+}-, cobalt^{2+}-, and manganese^{2+}-activated D-xylose isomerases. *Biochem. J. 278*, 285−292.
(23) Kersters-Hilderson, H., Callens, M., Van Opstal, O., Vangrysperre, W., and De Bruyne, C. K. (1987) Kinetic characterization of D-xylose isomerases by enzymic assays using D-sorbitol dehydrogenase. *Enzyme Microb. Technol. 9*, 145−148.
(24) Farber, G. K., Glasfeld, A., Tiraby, G., Ringe, D., and Petsko, G. A. (1989) Crystallographic studies of the mechanism of xylose isomerase. *Biochemistry 28*, 7289−7297.
(25) Whitaker, R. D., Cho, Y., Cha, J., Carrell, H. L., Glusker, J. P., Karplus, P. A., and Batt, C. A. (1995) Probing the roles of active site residues in D-xylose isomerase. *J. Biol. Chem. 270*, 22895−22906.
(26) Amyes, T. L., O'Donoghue, A. C., and Richard, J. P. (2001) Contribution of phosphate intrinsic binding energy to the enzymatic rate acceleration for triosephosphate isomerase. *J. Am. Chem. Soc. 123*, 11325−11326.
(27) Trentham, D. R., McMurray, C. H., and Pogson, C. I. (1969) The active chemical state of D-glyceraldehyde 3-phosphate in its reactions with D-glyceraldehyde 3-phosphate dehydrogenase, aldolase and triose phosphate isomerase. *Biochem. J. 114*, 19−24.
(28) Allen, K. N., Lavie, A., Petsko, G. A., and Ringe, D. (1995) Design, Synthesis, and Characterization of a Potent Xylose Isomerase Inhibitor, D-Threonohydroxamic Acid, and High-Resolution X-ray Crystallographic Structure of the Enzyme-Inhibitor Complex. *Biochemistry 34*, 3742−3749.
(29) Glasoe, P. K., and Long, F. A. (1960) Use of glass electrodes to measure acidities in deuterium oxide. *J. Phys. Chem. 64*, 188−190.
(30) Callens, M., Kersters-Hilderson, H., Vandekerckhove, J., Van Opstal, O., and De Bruyne, C. K. (1985) Purification and some physicochemical properties of D-xylose isomerase from *Streptomyces violaceus-ruber*. *Biochem. Int. 11*, 467−475.
(31) Otwinowski, Z., and Minor, W. (1997) Processing of X-ray diffraction data collected in oscillation mode. *Methods Enzymol. 276*, 307−326.
(32) Ramagopal, U. A., Dauter, M., and Dauter, Z. (2003) SAD manganese in two crystal forms of glucose isomerase. *Acta Crystallogr. D59*, 868−875.
(33) Kissinger, C. R., Gehlhaar, D. K., and Fogel, D. B. (1999) Rapid automated molecular replacement by evolutionary search. *Acta Crystallogr. D55*, 484−491.
(34) Brunger, A. T., Adams, P. D., Clore, G. M., DeLano, W. L., Gros, P., Grosse-Kunstleve, R. W., Jiang, J. S., Kuszewski, J., Nilges, M., Pannu, N. S., Read, R. J., Rice, L. M., Simonson, T., and Warren, G. L. (1998) Crystallography & NMR system: A new software suite for macromolecular structure determination. *Acta Crystallogr. D54*, 905−921.
(35) Sheldrick, G. M. (2008) A short history of SHELX. *Acta Crystallogr. A64*, 112−122.
(36) Emsley, P., and Cowtan, K. (2004) Coot: Model-building tools for molecular graphics. *Acta Crystallogr. D60*, 2126−2132.
(37) Amyes, T. L., and Richard, J. P. (1996) Determination of the pK_a of ethyl acetate: Brønsted correlation for deprotonation of a simple oxygen ester in aqueous solution. *J. Am. Chem. Soc. 118*, 3129−3141.
(38) O'Donoghue, A. C., Amyes, T. L., and Richard, J. P. (2005) Hydron Transfer Catalyzed by Triosephosphate Isomerase. Products of Isomerization of (R)-Glyceraldehyde 3-Phosphate in D_2O. *Biochemistry 44*, 2610−2621.
(39) Go, M. K., Malabanan, M. M., Amyes, T. L., and Richard, J. P. (2010) Bovine Serum Albumin-Catalyzed Deprotonation of [1-^{13}C]-Glycolaldehyde: Protein Reactivity toward Deprotonation of the α-Hydroxy α-Carbonyl Carbon. *Biochemistry 49*, 7704−7708.
(40) Jencks, W. P. (1975) Binding energy, specificity and enzymic catalysis: The Circe effect. *Adv. Enzymol. Relat. Areas Mol. Biol. 43*, 219−410.
(41) Alahuhta, M., and Wierenga, R. K. (2010) Atomic resolution crystallography of a complex of triosephosphate isomerase with a reaction intermediate analog: New insight in the proton transfer reaction mechanism. *Proteins: Struct., Funct., Bioinf. 78*, 1878−1888.
(42) Zhang, Z., Sugio, S., Komives, E. A., Liu, K. D., Knowles, J. R., Petsko, G. A., and Ringe, D. (1994) Crystal Structure of Recombinant Chicken Triosephosphate Isomerase-Phosphoglycolohydroxamate Complex at 1.8-Å Resolution. *Biochemistry 33*, 2830−2837.
(43) Collyer, C. A., Henrick, K., and Blow, D. M. (1990) Mechanism for aldose-ketose interconversion by D-xylose isomerase involving ring opening followed by a 1,2-hydride shift. *J. Mol. Biol. 212*, 211−235.
(44) Schray, K. J., and Rose, I. A. (1971) Anomeric specificity and mechanism of two pentose isomerases. *Biochemistry 10*, 1058−1062.
(45) Bogumil, R., Kappl, R., Huettermann, J., and Witzel, H. (1997) Electron Paramagnetic Resonance of D-Xylose Isomerase: Evidence for Metal Ion Movement Induced by Binding of Cyclic Substrates and Inhibitors. *Biochemistry 36*, 2345−2352.
(46) Kovalevsky, A. Y., Hanson, L., Fisher, S. Z., Mustyakimov, M., Mason, S. A., Trevor Forsyth, V., Blakeley, M. P., Keen, D. A., Wagner, T., Carrell, H. L., Katz, A. K., Glusker, J. P., and Langan, P. (2010) Metal Ion Roles and the Movement of Hydrogen during Reaction Catalyzed by D-Xylose Isomerase: A Joint X-ray and Neutron Diffraction Study. *Structure (Cambridge, MA, U.S.) 18*, 688−699.
(47) Drew, K. N., Zajicek, J., Bondo, G., Bose, B., and Serianni, A. S. (1998) ^{13}C-labeled aldopentoses: Detection and quantitation of cyclic and acyclic forms by heteronuclear 1D and 2D NMR spectroscopy. *Carbohydr. Res. 307*, 199−209.
(48) Tsang, W.-Y., Amyes, T. L., and Richard, J. P. (2008) A substrate in pieces: Allosteric activation of glycerol 3-phosphate dehydrogenase (NAD$^+$) by phosphite dianion. *Biochemistry 47*, 4575−4582.
(49) Go, M. K., Amyes, T. L., and Richard, J. P. (2010) Rescue of K12G Triosephosphate Isomerase by Ammonium Cations: The Reaction of an Enzyme in Pieces. *J. Am. Chem. Soc. 132*, 13525−13532.
(50) Street, I. P., Rupitz, K., and Withers, S. G. (1989) Fluorinated and Deoxygenated Substrates as Probes of Transition-State Structure in Glycogen Phosphorylase. *Biochemistry 28*, 1581−1587.
(51) Richard, J. P., McCall, D. A., Heo, C. K., and Toteva, M. M. (2005) Ground-State, Transition-State, and Metal-Cation Effects of the 2-Hydroxyl Group on β-D-Galactopyranosyl Transfer Catalyzed by β-Galactosidase (*Escherichia coli*, lac Z). *Biochemistry 44*, 11872−11881.
(52) Katz, A. K., Li, X., Carrell, H. L., Hanson, B. L., Langan, P., Coates, L., Schoenborn, B. P., Glusker, J. P., and Bunick, G. J. (2006)

Locating active-site hydrogen atoms in D-xylose isomerase: Time-of-flight neutron diffraction. *Proc. Natl. Acad. Sci. U.S.A. 103*, 8342−8347.
(53) Kovalevsky, A. Y., Katz, A. K., Carrell, H. L., Hanson, L., Mustyakimov, M., Fisher, S. Z., Coates, L., Schoenborn, B. P., Bunick, G. J., Glusker, J. P., and Langan, P. (2008) Hydrogen Location in Stages of an Enzyme-Catalyzed Reaction: Time-of-Flight Neutron Structure of D-Xylose Isomerase with Bound D-Xylulose. *Biochemistry 47*, 7595−7597.
(54) Carrell, H. L., Glusker, J. P., Burger, V., Manfre, F., Tritsch, D., and Biellmann, J. F. (1989) X-ray analysis of D-xylose isomerase at 1.9 Å: Native enzyme in complex with substrate and with a mechanism-designed inactivator. *Proc. Natl. Acad. Sci. U.S.A. 86*, 4440−4444.
(55) Cleland, W. W., Frey, P. A., and Gerlt, J. A. (1998) The Low Barrier Hydrogen Bond in Enzymatic Catalysis. *J. Biol. Chem. 273*, 25529−25532.
(56) Gerlt, J. A., Kreevoy, M. M., Cleland, W. W., and Frey, P. A. (1997) Understanding enzymic catalysis: The importance of short, strong hydrogen bonds. *Chem. Biol. 4*, 259−267.
(57) Van Bastelaere, P. B. M., Kersters-Hilderson, H. L. M., and Lambeir, A.-M. (1995) Wild-type and mutant D-xylose isomerase from *Actinoplanes missouriensis*: Metal-ion dissociation constants, kinetic parameters of deuterated and non-deuterated substrates and solvent-isotope effects. *Biochem. J. 307*, 135−142.
(58) Lee, C., Bagdasarian, M., Meng, M., and Zeikus, J. G. (1990) Catalytic mechanism of xylose (glucose) isomerase from *Clostridium thermosulfurogenes*. Characterization of the structural gene and function of active site histidine. *J. Biol. Chem. 265*, 19082−19090.
(59) Rangarajan, M., and Hartley, B. S. (1992) Mechanism of D-fructose isomerization by *Arthrobacter* D-xylose isomerase. *Biochem. J. 283*, 223−233.
(60) Kraulis, P. J. (1991) MOLSCRIPT: A program to produce both detailed and schematic plots of protein structures. *J. Appl. Crystallogr. 24*, 946−950.
(61) Fenn, T. D., Ringe, D., and Petsko, G. A. (2003) POVScript+: A program for model and data visualization using persistence of vision ray-tracing. *J. Appl. Crystallogr. 36*, 944−947.